CEAS Space Journal (2023) 15:947–958
https://doi.org/10.1007/s12567-023-00499-8

ORIGINAL PAPER

Linearly combined transition model based on empirical spot growth correlations

Maximilian Karsch[1] · Jeroen Van den Eynde[2] · Johan Steelant[2]

Received: 15 February 2023 / Revised: 17 April 2023 / Accepted: 25 April 2023 / Published online: 9 May 2023

Abstract
The transition from laminar to turbulent flow in a hypersonic boundary layer is modeled using an intermittency-based linear combination approach. A simplified transition model like this enables a quick assessment of aero-thermal loads and the overall flight efficiency of high-speed vehicles during the initial design phase by weighting purely laminar and turbulent flow results on the basis of an empirically calculated intermittency. The transition model presented within this work includes an empirical model to account for Mach number, Reynolds number, wall temperature and pressure gradient effects on turbulent spot growth based on available turbulent spot studies in the literature. A validation of the transition model is carried out for a number of different test cases and a methodology to extend the model to generic geometries is presented to enable a more general application.

Keywords High-speed transition modeling · Turbulent spot growth · Compressibility · Wall temperature

1 Introduction

The process of laminar to turbulent boundary layer transition has important implications on the aerodynamic behavior, the structural heating and the overall flight efficiency of high-speed vehicles. Although being studied for over a century, the concept of boundary layer transition is not fully understood and a universal method to accurately predict both onset and extent of transition is not available.

To avoid dealing with transition or to apply a conservative approach, one may think of assuming a fully turbulent boundary layer on the whole vehicle to calculate the occurring aero-thermal loads. However, this would lead to much heavier vehicle concepts, compromising the maximum available payload significantly. An illustration of this matter was given in the context of the NASP program where a relative payload increase of 60–70% compared to the fully turbulent condition was estimated [1]. Likewise, it was also found that the vehicle take-off weight can vary by a factor of two or more depending on the estimated transition location [2]. The latter involves another popular engineering approach namely to estimate a fixed transition location based on empirical correlations and use turbulent calculations downstream. This disregards the finite extent of the transitional region and also implies a discontinuous distribution of the heat-transfer coefficient as the boundary layer switches from laminar to turbulent instantaneously. Both approaches were found to be unsatisfactory, in particular with respect to hypersonic flight where the laminar flow region as well as the transition zone itself can be quite extensive and may occupy large portions of the vehicle. Starting at the transition onset location, the rate and, consequently, the extent of the transitional region itself are governed by the individual growth and merger of turbulent spots.

Several transition models have been proposed in the past where the most promising ones include the concept of intermittency, a field variable which essentially describes the time fraction of the flow being turbulent at a certain location within the transitional zone. According to Narasimha [3], these models may be classified into the following four types

✉ Maximilian Karsch
maximilian.karsch@itv.uni-stuttgart.de

Jeroen Van den Eynde
Jeroen.Van.den.Eynde@esa.int

Johan Steelant
Johan.Steelant@esa.int

[1] Institute of Aerospace Thermodynamics, University of Stuttgart, Pfaffenwaldring 31, 70569 Stuttgart, Germany

[2] Flight Vehicles and Aerothermodynamics Engineering Section, ESA-ESTEC, Keplerlaan 1, 2200 AZ Noordwijk, The Netherlands

based on their level of complexity: (a) Integral methods, (b) Algebraic models, (c) Differential equation models and (d) Direct methods. An overview of early transition models according to this classification was given by Narasimha and Dey [4].

The first and simplest class is described by integral methods in which the currently proposed linearly combined model belongs to. Introduced by Emmons [5], the underlying idea is that laminar and turbulent flow are calculated independently from each other, e.g., using two separate sets of Reynolds-averaged Navier–Stokes (RANS) equations. The mean flow within the transitional region is then reconstructed by blending purely laminar and turbulent flow components using the intermittency as a weighting parameter. In this context, the intermittency factor itself is typically determined by a simple analytical expression. Transition models of this type have been proposed by Dhawan and Narasimha [6], Solomon et al. [7] and Chen and Thyson [8]. Algebraic transition models use a single set of RANS equations but use an intermittency-scaled eddy viscosity to model a gradual release of turbulence throughout the transition region. Examples for transition models of this class are given by Adams [9] who used an analytical expression for the intermittency distribution and Cebeci and Smith [10].

Higher-level transition models typically introduce an additional differential equation describing the intermittency transport. Steelant and Dick [11–13] used the concept of conditional averaging to derive two sets of equations, one for the laminar and one for the turbulent part of the flow which are coupled through the intermittency. Within this approach, laminar–turbulent interactions are included; however, the computational effort is effectively doubled. Therefore, efforts were made, e.g., by Suzen and Huang [14] and Cho and Chung [15] to combine the two sets of equations into a single RANS equation set. Another pressing issue was the usage of integral boundary layer parameters in the models which are not locally accessible. Langtry and Menter addressed these aspects in their γ-$Re_{\theta t}$ transition model [16, 17] by introducing two transport equations for the intermittency and the transition onset Reynolds number based on local flow variables. These are solved together with a single set of RANS equations and a modified version of the SST k - ω turbulence model. The recently proposed γ-α transition model by Van den Eynde and Steelant [18, 19] uses a similar approach but includes mechanisms of turbulent spot growth to model the intermittency production and is completely decoupled from the applied turbulence model. It has shown promising potential in predicting hypersonic boundary layer transition with and without pressure gradients. Direct numerical simulations (DNS) are inherently capable of calculating transitional flow as the full Navier–Stokes equations are considered, however, the large computational effort needed to resolve the smaller scales of the flow make them unfeasible for most practical engineering applications. Nevertheless, direct methods are often used to investigate detailed features of the transition process, e.g., the growth and propagation of a single turbulent spot.

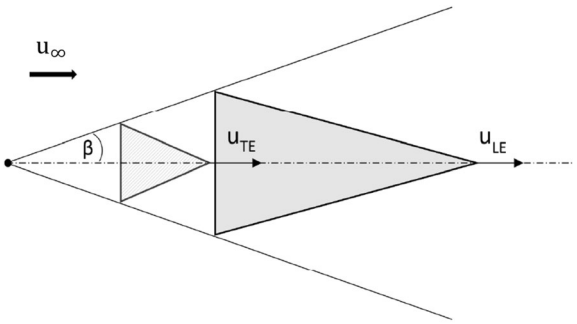

Fig. 1 Turbulent spot geometry

In this work, boundary layer transition is modeled using a simple linear combination approach. Similar to the γ- and γ-α model [11–13, 18, 19], the aim is to incorporate mechanisms of turbulent spot growth to reconstruct the intermittency evolution throughout the transitional region. Therefore, empirical correlations are presented that aim to reproduce the effects of compressibility, temperature and Reynolds number on the propagation and growth of individual turbulent spots. As these correlations describe the process of spot growth from a phenomenological point of view, they are thought to be useful in a more general context as well, e.g., for high-level transition models that use an intermittency-based approach.

2 Empirical correlations for turbulent spot growth

As the production, growth and propagation of turbulent spots represent the key mechanisms after breakdown, they need to be reproduced accordingly in the transition model to accurately predict the transition zone extent. In a plan view, the geometry of an individual spot may be represented in a simplified manner by a downstream pointing triangle as shown in Fig. 1. The concept of concentrated breakdown which was established by Narasimha [20] states that turbulent spots are generated at a certain streamwise location Re_{xt}. After the initial generation phase, turbulent spots approximately grow in a linear fashion as they propagate downstream until they eventually merge and form a fully turbulent boundary layer. While the rear of the spot moves with a velocity of u_{TE}, the spot front travels at a higher velocity u_{LE} which causes the spot to grow in the longitudinal direction. Further, the growth in the lateral direction is typically described with the

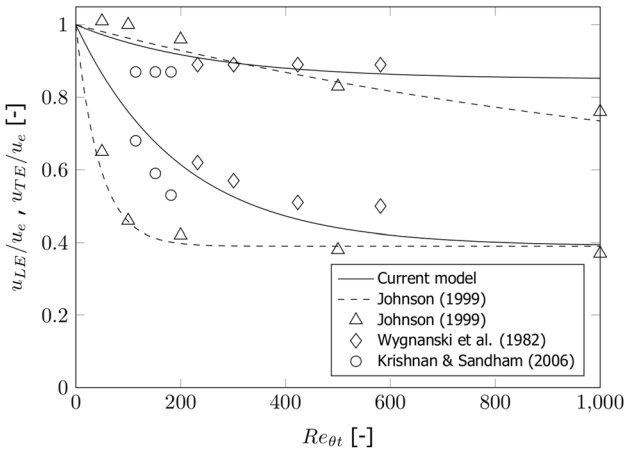

Fig. 2 Spot propagation velocities

spreading angle β formed between the symmetry line and the wing tip of the spot.

2.1 Spot propagation velocities

The spot propagation velocities have been reported to be a function of the Reynolds number within several studies found in literature. For instance, Wygnanski et al. [21] observed a decrease of the trailing edge velocity from 62% to 50% of the free-stream velocity in their experiments if the Reynolds number at the spot inception location was increased from $Re_\theta \approx 230$ to $Re_\theta \approx 580$. On the other hand, the leading edge velocity remained constant at 89% of the free-stream velocity.

In a numerical study, Johnson [22] also found inhibited spot growth at low Reynolds numbers which he attributed to the presence of strong viscous damping. Compared to the results of Wygnanski et al. [21] however, the decrease of the trailing edge velocity with increasing Reynolds number occurred more rapidly. Based on his obtained numerical results, Johnson also proposed correlations for the spot propagation velocities which are included in Fig. 2 for zero-pressure gradient flow along with other spot data and the currently proposed correlations. As the decrease of the propagation velocities observed by Johnson was found to be too large, the correlations given in Ref. [22] for zero-pressure gradient flow are modified to

$$\frac{u_{LE}}{u_e} = 0.15\exp(-0.004\,Re_{\theta t}) + 0.85 \tag{1}$$

and

$$\frac{u_{TE}}{u_e} = 0.61\exp(-0.005\,Re_{\theta t}) + 0.39 \tag{2}$$

to obtain a better agreement with present experimental data although it is somewhat unclear which dataset is most representative. The used Reynolds number is defined based on the momentum thickness at the transition onset location according to the experimental and numerical data where the Reynolds number is typically specified at the spot inception point. Moreover, it is important to mention that measurements of spot propagation velocities are extremely sensitive with respect to the applied methodology. More precisely, a threshold criterion to define the turbulent/non-turbulent interface is required which differs among different spot studies. This is potentially a major cause of the scatter seen within the experimental and numerical data. In this context, a general convention to define the shape and extremities of turbulent spots is needed to enable a better comparison of spot growth data.

Apart from the scatter, the understanding of the full dependencies of the spot convection velocities is still incomplete and also requires further investigation. A number of studies, e.g., Refs. [22–25], addressed the effect of favorable and adverse pressure gradients. In a recent work, Van den Eynde and Steelant [26] proposed an empirical correlation of the spot propagation velocities as a function of the Mach number.

2.2 Lateral spreading rate

Similar to the longitudinal spot growth, the lateral growth rate of turbulent spots has also been subject of several experimental and numerical studies in the past. A study by Fischer [27] who collected spreading rates of turbulent disturbances such as turbulent spots, wedges and jets revealed a strong Mach number effect on the lateral spreading resulting in a growth rate reduction by a factor of three at $M_\infty = 5$. This trend has been widely accepted and further confirmed with more recent results. However, quantifying this effect remains a challenge due to the scarcity of hypersonic results and the large scatter found in the data. Again, the latter is most likely related to different spot shape definitions. Further, experimental measurements by Chong and Zhong [28] on the three-dimensional structure of turbulent spots indicated the presence of a lateral overhang beneath the wing tip region of the spot. Based on this observation, consistently lower spreading angles should be expected for heat-transfer measurements at the wall compared to other measurement techniques such as hot-wire anemometry which are applied at a certain distance away from the wall. Regarding the driving mechanism behind the lateral growth, Gad-El-Hak [29] found that the lateral turbulence spreading principally occurs through a destabilization mechanism of the surrounding laminar boundary layer in addition to the classical turbulent entrainment mechanism. The mechanism was investigated in more detail within a numerical study by Redford et al. [30]

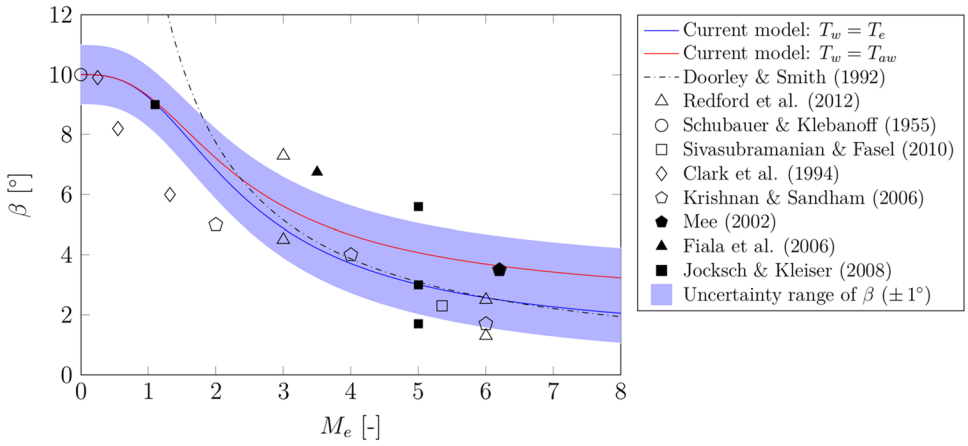

Fig. 3 Lateral spot spreading angle. To account for potential measurement uncertainties in the numerical and experimental studies, a shaded area is added where $\beta(T_w = T_e) - 1°$ and $\beta(T_w = T_{aw}) + 1°$ constitute the lower and upper bound, respectively

which revealed the presence of lateral jets emanating from the wingtip region of the spots. This observation motivated Sandham [31] to formulate a convective Mach number for the lateral growth of turbulent spots in analogy to the growth rate of turbulent mixing layers as

$$M_c = M_e \frac{1 - u_{jet}/u_e}{1 + \sqrt{T_{jet}/T_e}}, \tag{3}$$

where the subscript $(\cdot)_{jet}$ denotes the corresponding variable taken at the lateral jet location. The convective Mach number is used in the current work to encompass Mach number and temperature effects on turbulent spot growth within the transition model. While the streamwise velocity at the jet location is estimated with $u_{jet} \approx 0.45\, u_e$, the temperature ratio is approximated using the modified Crocco-Busemann relation

$$\frac{T_{jet}}{T_e} = 0.45 + 0.55\,\frac{T_w}{T_e} + 0.25\, r\,\frac{\kappa - 1}{2} M_e^2 \tag{4}$$

with the recovery factor r. The temperature effect on spot growth has been addressed in numerical studies, e.g., by Redford et al. [30] and Jocksch and Kleiser [32]. Overall, it was shown that the wall temperature plays a secondary role and that a cooled wall generally yields lower spreading angles. Besides the Mach number and temperature effect, the spreading angle is also reported to be a weak function of the Reynolds number, e.g., by Schubauer and Klebanoff [33] or Wygnanski et al. [21] with a slight reduction of β at lower Reynolds numbers. On the other hand, a numerical study by Jocksch and Kleiser [32] indicated a much stronger effect of the Reynolds number. Within the current model, the Reynolds number dependency is represented using a damping factor proposed by Johnson [22]. Regarding the convective Mach number dependency, an analytic function was fitted to the data given in Ref. [31] which in turn was obtained from linear stability theory. All in all, the current correlation for the lateral spot spreading angle reads

$$\frac{\beta}{\beta_0} = f_1(M_c) f_2(Re_{\theta t}) = \left(1 + 7.06\, M_c^{2.86}\right)^{-0.5} \left[1 - 0.29 \exp(-0.0035\, Re_{\theta t})\right], \tag{5}$$

where the incompressible reference value is $\beta_0 = 10°$ based on experimental results by Schubauer and Klebanoff [33]. The result for two different wall temperature conditions are plotted in Fig. 3 together with experimental and numerical results. Note that in this plot, the Reynolds number dependency is neglected, i.e., function f_2 from Eq. (5) is set to one. Within the current formulation, the stabilizing effect with respect to compressibility and wall cooling seems to be captured correctly. Additionally, it is interesting to note that the cold wall case is in quite good agreement with the theoretical model by Doorley and Smith [34] especially for $M_e > 5$. Given the model formulation of the spreading angle, one could argue that a more meaningful representation could be obtained by plotting directly over the convective Mach number rather than the edge Mach number. However, with the large scatter present in the dataset the trends are not clearly visible and no satisfactory collapse of the data could be achieved. A similar conclusion was drawn in a recent work by Van den Eynde and Steelant [26].

3 Methodology

The classical linear combination approach poses one of the simplest methods to model boundary layer transition and was found to provide an excellent description of the transition zone for two-dimensional flows with zero-pressure gradient [3]. In essence, the underlying hypothesis of this model states that laminar and turbulent flow components do not interact by any means and develop independently. Using Narasimha's near-wall intermittency distribution, the purely laminar and turbulent flow components are combined in a linear fashion with their corresponding portions through

$$St = (1-\gamma)\,St_{lam} + \gamma\,St_{turb} \tag{6}$$

to reconstruct a transitional Stanton number. The laminar and turbulent flow components are obtained from theoretical expressions or numerical solutions, while the intermittency is defined by

$$\gamma = \begin{cases} 1-\exp(-\hat{n}\sigma(Re_x - Re_{xt})^2) & , Re_x > Re_{xt} \\ 0 & , Re_x \le Re_{xt} \end{cases} \tag{7}$$

with the dimensionless spot production parameter $\hat{n}\sigma$ and the transition onset Reynolds number Re_{xt}. Different best-practice correlations exist that allow the estimation of R_{xt} based on, e.g., the free-stream turbulence level, Tu_∞, or the Mach number. Here, we will use different correlations for Re_{xt} depending on the validation test case as will be detailed in Sect. 4.

Based on the model of Steelant and Dick [11], and subsequent updated formulation by Van den Eynde and Steelant [18], the dimensionless spot production parameter is calculated according to

$$\hat{n}\sigma = c_1\,(Tu_\infty)^{c_2} f_\sigma f_K f_\gamma \tag{8}$$

with $c_1 = 1.25 \cdot 10^{-11}$ and $c_2 = 7/4$ taken from Mayle [35]. Further, several correction factors f are included in order to represent different effects on the spot production parameter $\hat{n}\sigma$. The empirical correlations for the leading edge velocity, the trailing edge velocity and the lateral spreading angle of the turbulent spot are combined to yield the relative spot growth parameter with

$$f_\sigma = \frac{\sigma}{\sigma_0} = \frac{1}{\sigma_0}\left(\frac{u_e}{u_{TE}} - \frac{u_e}{u_{LE}}\right)\tan(\beta) \tag{9}$$

according to Vinod and Govindarajan [36]. The reference value of $\sigma_0 = 0.25$ is obtained by evaluating the corresponding correlations at $M_c = 0$ and $Re_{\theta t} \to \infty$ to ensure $f_\sigma \le 1$. Unlike formulations within previous models, this approach establishes a direct link between the total spot production parameter $\hat{n}\sigma$ and the phenomenological description of the turbulent spot with its propagation parameters u_{LE}, u_{TE} and β.

To also account for streamwise pressure gradient effects, an additional correction factor from Steelant and Dick [11] is used which is defined by

$$f_K = \begin{cases} (474\,Tu_\infty^{-2.9})^{(1-\exp(2\cdot 10^6\,K))} & , K < 0 \\ 10^{-3227\,K^{0.5985}} & , K \ge 0, \end{cases} \tag{10}$$

where the pressure gradient parameter is calculated as

$$K = -\frac{\mu_\infty}{\rho_\infty^2\,u_\infty^3}\,|1-M_\infty^2|\,\frac{dp}{ds} \tag{11}$$

and dp/ds denotes the pressure gradient along the streamline.

The third correction factor f_γ incorporates the concept of distributed breakdown and is defined by

$$f_\gamma = \begin{cases} 1-\exp(-1.735\tan(5.45\,\gamma_{mod} - 0.95375) - 2.2) & , \gamma_{mod} < 0.45 \\ 1 & , \gamma_{mod} \ge 0.45 \end{cases} \tag{12}$$

according to Steelant and Dick [37]. A slightly modified argument with $\gamma_{mod} = \gamma + 0.01$ is used herein to exclude negative values for f_γ in the vicinity of x_t which would result in a negative intermittency production. The purpose of this correction factor is to gradually ramp up the spot production parameter $\hat{n}\sigma$ during the initial stage of transition which should enable the model to provide more realistic results.

It is important to mention that the analytic intermittency distribution from Eq. (7) represents an integrated formulation, i.e., it is valid for a constant spot production parameter $\hat{n}\sigma$. To allow for varying spot production throughout the domain, e.g., due to a spatially changing wall temperature, the differential formulation

$$\frac{1}{1-\gamma}\frac{d\gamma}{dx} = B(x) \quad \text{with} \quad B(x) = 2\,\hat{n}\sigma\frac{u^2}{\nu^2}(x - x_{tr}) \tag{13}$$

given in Ref. [11] is employed which yields

$$\gamma = 1 - \exp\left(-\int_{x_{tr}}^{x} B(x)\,dx\right) \quad , \quad x > x_{tr} \tag{14}$$

for the intermittency distribution. This formulation, along with the aforementioned correlations and modeling constants, will be applied for all test cases presented in this work. Note, however, that we also consider $f_\sigma = 1$ for the two incompressible test cases (T3A and T3B) shown in Sect. 4.

Before applying the presented model to a number of test cases, it is instructive to first investigate the sensitivity of the transition model with respect to compressibility and temperature effects as well as different free-stream turbulence levels. Therefore, intermittency distributions are calculated with Eq. (7) for different Mach numbers, wall temperature conditions and free-stream turbulence levels and are shown in Fig. 4. To display the effect on the intermittency evolution, $Re_x - Re_{xt}$ is treated as an independent variable. Figure 4a exhibits the effect of an increasing edge Mach number from three to five on the intermittency evolution for a fixed free-stream turbulence level of $Tu_\infty = 0.5\%$. For the sake of simplicity, the Reynolds number effect in this figure is neglected, i.e., Equations (1), (2) and (5) are evaluated at $Re_\theta \to \infty$ limit and a zero-pressure gradient flow with $f_K = 1$ is assumed. As the Mach number is increased, the transition rate decreases which in turn results in an extended transitional region. If the end of the transition is defined at $\gamma = 0.99$, this extent is quantified

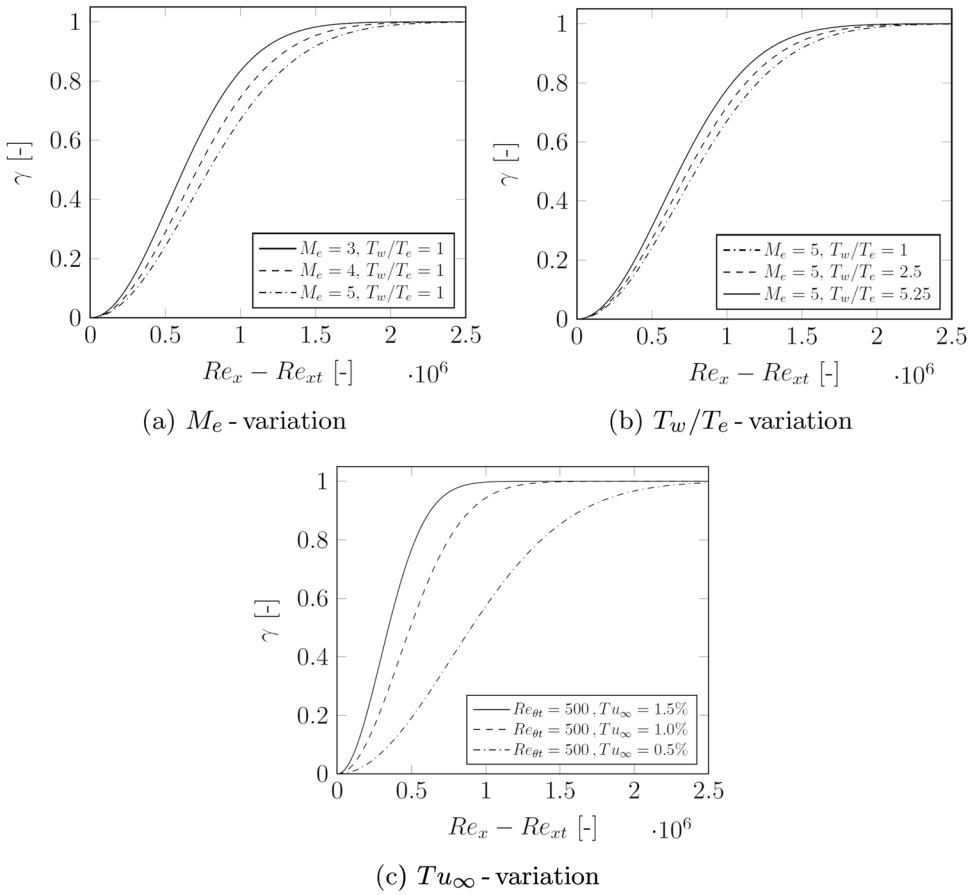

(a) M_e - variation (b) T_w/T_e - variation

(c) Tu_∞ - variation

Fig. 4 Sensitivity of intermittency distribution to Mach number, wall-to-edge temperature ratio and free-stream turbulence level

with $Re_{\Delta xt} = 1.6 \cdot 10^6$ at Mach three and $Re_{\Delta xt} = 2.04 \cdot 10^6$ at Mach five, respectively.

Likewise, a similar effect is noticed for wall cooling as shown in Fig. 4b for a constant Mach number of five. In this case, the transition zone increases from $Re_{\Delta xt} = 1.75 \cdot 10^6$ to $Re_{\Delta xt} = 2.04 \cdot 10^6$ if the wall temperature is decreased from the adiabatic wall temperature down to the boundary layer edge temperature. Note that, analogous to Fig. 4a, we assume $Tu_\infty = 0.5\%$, $f_K = 1$ and $Re_\theta \to \infty$. Lastly, we evaluate intermittency distributions for three different free-stream turbulence levels in Fig. 4c using a fixed transition onset point and zero-pressure gradient flow, i.e., $Re_{\theta t} = 500$ and $f_K = 1$.

Clearly, the shown distributions indicate a strong impact of Tu_∞ on the predicted transition rate where lower free-stream turbulence levels yield extended transition lengths which can be inferred based on Eq. (8). Here, the relationship $\hat{n}\sigma \propto (Tu_\infty)^{7/4}$ implies that $\hat{n}\sigma \to 0$ for $Tu_\infty \to 0$. Note that this behavior also applies to accelerating flows with $K \geq 0$ according to Eq. (10). For decelerating flows (i.e., $K < 0$), on the other hand, the trend of a decreasing spot production rate with respect to a decreasing free-stream turbulence level is reversed as pointed out by Steelant and Dick [11]. Here, the exponential function will evaluate to a number very close to zero for most cases because of the extremely small argument with $2 \cdot 10^6 K \ll 0$. The pressure gradient correction factor can thus be approximated by $f_K \approx 474\, Tu_\infty^{-2.9}$ which will overtake the aforementioned scaling of $\hat{n}\sigma \propto (Tu_\infty)^{7/4}$ contained in Eq. (8).

4 Validation

In the following, the proposed linearly combined transition model is applied to several flat plate test cases which include both hot and cold wall temperature conditions as well as incompressible and hypersonic flow.

4.1 T3 series

Several incompressible boundary layer transition experiments with varying free-stream turbulence levels were carried out by Roach and Brierley [38] on a flat plate and are used herein for comparisons with the results provided by the linearly combined transition model. The corresponding test conditions for the cases under consideration are summarized in Table 1.

Table 1 Test conditions of T3A and T3B case

Case	Tu_∞ [%]	u_∞ [m/s]	ρ_∞ [kg/m^3]	Re_u [1/m]	T_w/T_e [–]
T3A	3	5.4	1.2	$3.60 \cdot 10^5$	1
T3B	6	9.4	1.2	$6.27 \cdot 10^5$	1

To predict the transition onset, we use a correlation proposed by Mayle [35] with

$$Re_{\theta t} = 420\, Tu_\infty^{-0.69}, \tag{15}$$

which corresponds to

$$Re_{xt} = \left(\frac{Re_{\theta t}}{0.664}\right)^2 \tag{16}$$

assuming a Blasius profile. The free-stream turbulence level ranges from $Tu_\infty = 3\,\%$ up to $Tu_\infty = 6\,\%$ with very low free-stream velocities, u_∞, and $T_w = T_e$. Hence, neither Mach number nor wall temperature effects on turbulent spot growth come into effect. Further, both cases represent experiments on flat plates with zero-pressure gradient flow, i.e., $f_K = 1$.

Based on the experimental results, the measured transition lengths are rather short which suggest that the transition process is mainly driven by the high turbulence level rather than the development of individual turbulent spots. To investigate this hypothesis, we also consider a variation of our proposed model where we set the spot correction factor to unity, i.e., $f_\sigma = 1$. This implies that the spot production parameter $\hat{n}\sigma$ according to Eq. (8) only depends on the free-stream turbulence level. In other words, the Reynolds number effect on turbulent spot growth is neglected using this approach. In addition, the laminar and turbulent flow components required to reconstruct a transitional distributions are calculated analytically using classical expressions from boundary layer theory. In particular, the laminar component for the skin friction coefficient $c_{f,lam}$ is obtained from the Blasius solution. Respectively, a classical empirical correlation with $c_{f,turb} = 0.0576\, Re_{xt}^{-1/5}$ is employed for the turbulent counterpart. The resulting skin friction distribution from the linearly combined transition model for the T3A case is shown in Fig. 5 together with the experimental data as well as the fully laminar and turbulent components.

Using the proposed variation of our transition model with $f_\sigma = 1$, a reasonable description of the transitional zone is obtained and the transition rate is captured quite well, while the transition onset location is predicted a bit too early. If the Reynolds number effect is included, an increased value for the spot trailing edge celerity with $u_{TE} = 0.62\, u_e$ rather than $u_{TE} = 0.39\, u_e$ is found due to

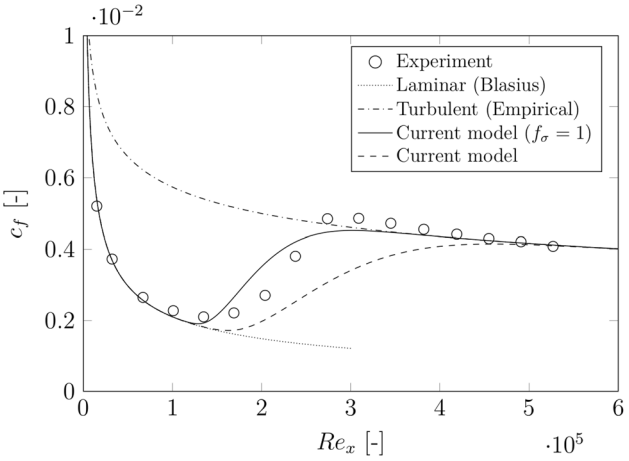

Fig. 5 Skin friction coefficient for T3A test case

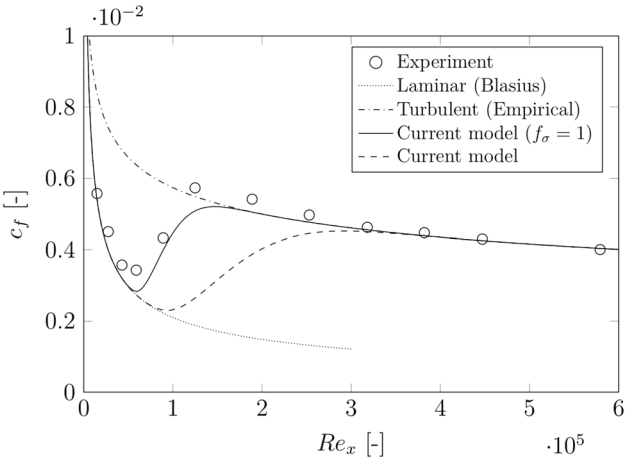

Fig. 6 Skin friction coefficient for T3B test case

the early transition onset at $Re_{\theta t} \approx 200$. This results in a quite low value for the spot growth correction factor with $f_\sigma = 0.32$ and consequently, in a largely extended transition zone as indicated by the dashed line in Fig. 5. As the current model assumes both laminar and turbulent flow to start from the leading edge of the plate, it is inherently incapable of predicting the overshoot effect. This clearly poses a crucial limitation of the presented linearly combined model.

The corresponding results for the T3B case are given in Fig. 6 and show a reasonable agreement with the experiment if $f_\sigma = 1$ is assumed. Taking the Reynolds number effect on the spot trailing edge celerity u_{TE} into account leads again to a very low transition rate which is not supported by the experimental data. Compared to the T3A case, an earlier onset as well as a shorter transition length

Table 2 Test conditions of selected RWG-M6 cases

Case	M_e [–]	p_0 [bar]	T_0 [K]	Re_u [1/m]	T_w/T_e [–]
RWG-M6	5.98	12.94	548.8	$9.44 \cdot 10^6$	4.42
RWG-M6-SWBLI	5.98	13.15	511.4	$10.77 \cdot 10^6$	4.74

due to an elevated free-stream turbulence level is correctly reproduced by the current model.

4.2 RWG-M6 series

Two hypersonic flat plate experiments of the RWG-M6 series, carried out at the Ludwieg-Tube Facility DNW-RWG at DLR Göttingen, were used as validation test cases. A summary of the test conditions is given in Table 2 and are taken directly from the experimental report [39].

The RWG-M6 case describes a Mach 6 zero-pressure gradient flow without shock impingement. To calculate the laminar and turbulent component of the transitional Stanton number distribution, theoretical expressions are used in this case. In particular, the Chapman–Rubesin approximation in combination with the reference temperature concept by Eckert [40] is used for the laminar distribution; whereas, an analytical description by White and Christoph [40] is used for the turbulent component.

Regarding the transition onset Reynolds number, a correlation by Steelant and Dick [13] is used in combination with a compressibility factor given in Ref. [3] to yield

$$Re_{xt} = (400\,094\, Tu_\infty^{-1.38} - 105\,254\, Tu_\infty^{-7/8})(1 + 0.38\, M_e^{0.6}) \,. \tag{17}$$

Unfortunately, no free-stream turbulence levels are reported for the RWG-M6 series; however, a value for the Tu_∞ is required within the current transition model to calculate the onset location and transition rate. Therefore, the transition onset correlation from Eq. (17) is solved inversely with the experimentally measured onset Reynolds number which yields a turbulence level of approximately 0.5%. This ranks slightly below the values given in Ref. [18], where 0.6–0.7% was estimated for the same case. Further, the transition onset Reynolds number based on the momentum thickness which is needed within the spot growth correlations is calculated by applying the reference temperature concept to a Blasius profile using

$$Re_{\theta t} = 0.664 \sqrt{Re_{xt}\, C^\star}, \tag{18}$$

where $C^\star$ denotes the Chapman–Rubesin parameter. The corresponding result of the transition model is shown in Fig. 7 together with experimental data and numerical results obtained with the γ-α model and the Langtry–Menter γ-$Re_{\theta t}$ transition model. For the latter, an extended version

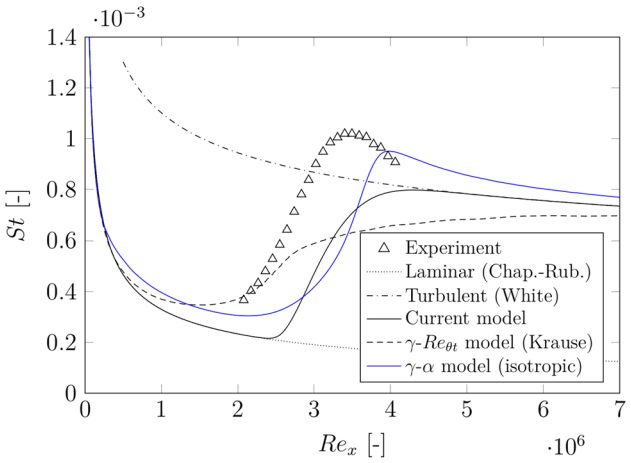

Fig. 7 Stanton number distribution for RWG-M6 test case

according to Krause et al. [41, 42] is employed which is also shown in Ref. [18]. Although this extension is particularly designed for hypersonic flow it is clearly not able to correctly reproduce the transition rate and peak Stanton number observed in the experiments. On the other hand, the current transition model seems to capture the transition rate quite well. A crucial limitation of the current model in the given configuration is that it cannot replicate the typical overshoot effect at the end of transition indicated by the experimental data since it is bound between the laminar and turbulent Stanton number distribution. To account for this, the virtual origin of the turbulent flow component could be taken at the transition onset location rather than the leading edge of the plate which was shown in a recent study by Raghunath et al. [43]. However, an attempt like this is not part of the current work as it is difficult to transfer this concept to generic geometries. The γ-α model is able to capture both the peak Stanton number and the transition rate quite well but the transitional overshoot is predicted somewhat further downstream.

The second considered test case of the RWG-M6 series includes a shock-wave boundary layer interaction created by an oblique shock wave which impinges the boundary layer near the end of transition. In this case, the laminar and turbulent component for the transitional Stanton number are created with the unstructured CFD solver TAU by Deutsches Zentrum für Luft- und Raumfahrt (DLR) using prismatic cells near the wall and tetrahedral cells otherwise. Regarding the turbulent computation, the classical Menter SST k-ω -model was used as a turbulence model.

Before examining the resulting transitional Stanton number distribution, the impact of the pressure gradient on the intermittency distribution is shown in Fig. 8 based on the laminar CFD solution. It can be inferred that the large adverse pressure gradient found around the impingement

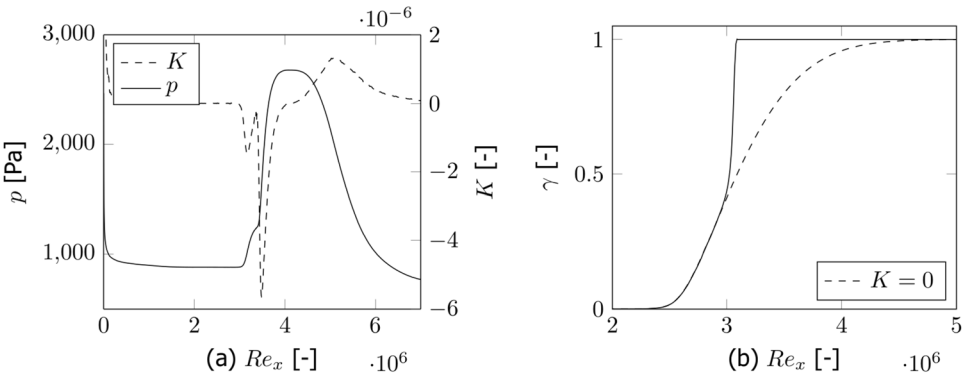

Fig. 8 Pressure distribution and pressure gradient parameter (left) and intermittency distribution (right) for RWG-M6-SWBLI case

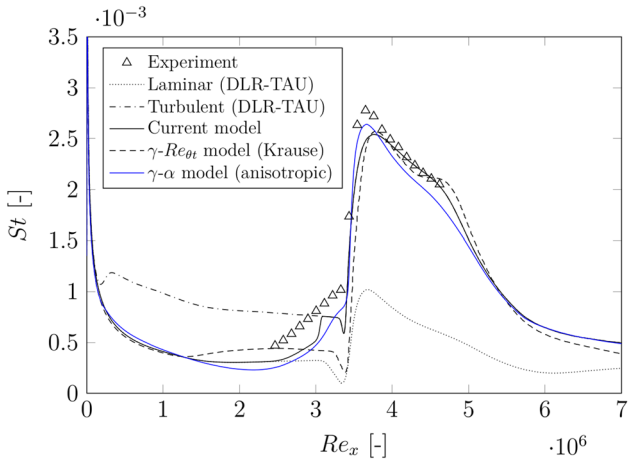

Fig. 9 Stanton number distribution for RWG-M6-SBLI case

location results in a steep increase in the intermittency which immediately yields a fully turbulent flow state that is retained downstream. This is in line with numerical and experimental observations that showed greatly enhanced spot growth for adverse pressure gradients, e.g., Ref. [22] or [24].

The corresponding result for the Stanton number distribution is shown in Fig. 9 together with numerical results with the extended γ-$Re_{\theta t}$ transition model and the γ-α model. The same methodology has been applied with respect to Re_{xt}, effectively matching the onset location to the experiment. The plot shows that the peak Stanton number is captured best by the γ-α model followed by the γ-$Re_{\theta t}$ and the current model. Further, unsatisfactory results are obtained with the γ-$Re_{\theta t}$ upstream of the shock impingement location as the onset is predicted too early and the gradual increase of St_{exp} in this region is not reproduced. On the other hand, the current model as well as the γ-α predict the early transition rate much better although the absolute values are still lower compared to the experiment.

Table 3 Test conditions of selected ATLLAS-II cases

Case	M_e [–]	p_0 [bar]	T_0 [K]	Re_u [1/m]	T_w/T_e [–]
Cold wall	7.4	31.54	2687	$6.65 \cdot 10^6$	1.13
Hot wall	7.4	31.54	2687	$6.65 \cdot 10^6$	2.68

4.3 ATLLAS-II series

In addition to the RWG-M6 series, the transition model is also applied to two selected test cases that were carried out at the High Enthalpy Shock Tunnel Göttingen (HEG) as part of the ATLLAS-II project.[1] The corresponding test conditions are summarized in Table 3 and are taken from the experimental report [44].

Two flat plate cases with zero-pressure gradient flow are considered differing only with respect to their wall temperature condition. While the first case represents a cold wall at $T_w = 295$ K, the wall temperature of the second case is significantly higher with $T_w > 700$ K. Further, the experimental report [44] provides estimates for the spot production parameters with $\hat{n}\sigma_{cold} = 6.66 \cdot 10^{-13}$ and $\hat{n}\sigma_{hot} = 7.78 \cdot 10^{-13}$ which are obtained based on a fit to experimental data. This yields a relative increase between the cold and hot wall of about 17% for the spot production parameter. The current model suggest a lower impact of the wall temperature with a relative increase of about 8%. The resulting Stanton number distributions are given in Fig. 10.

The purely laminar and turbulent flow components for the reconstruction of the transitional Stanton number are determined using the same analytical expressions from boundary layer theory as in the RWG-M6 case. Again values the free-stream turbulence level are not directly available, however, an estimate of 0.6% is given in the experimental report which is adopted within the current work. Further, it is important to mention that the onset Reynolds number Re_{xt} is chosen

[1] https://www.esa.int/Enabling_Support/Space_Engineering_Technology/ATLLAS_II_-_Project_summary.

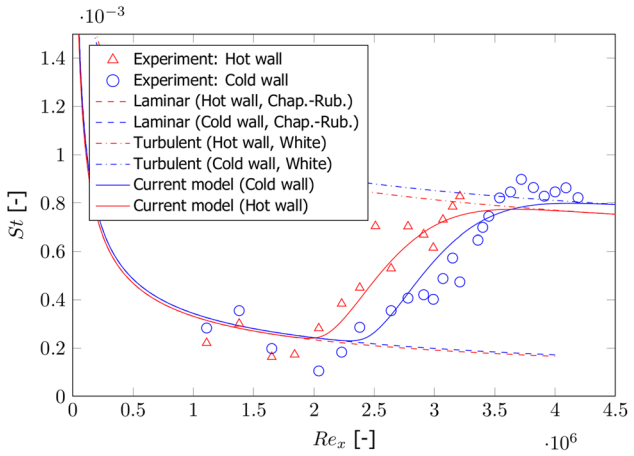

Fig. 10 Stanton number distribution for ATLLAS-II test cases

to match with the experimental onset point for both cases. The onset correlation from Eq. (17) predicts an early transition with $Re_{xt} = 1.46 \cdot 10^6$ for both cases as the effect of wall temperature is not included. Incorporating this effect is quite complex because it depends on the prevalent instability mode and thus, is not easily reproducible within a simple correlation. Here, the experimental Stanton number distributions indicate an earlier start of transition for the hot wall case. The current transition model is able to reproduce the experimentally measured Stanton number distributions reasonably well although it is difficult to infer the impact of the wall temperature on the transition rate using this representation.

5 Application to hypersonic flight vehicle

A boundary layer tool developed by Hoffmann et al. [45] has been extended as part of this work by means of implementing the currently proposed linearly combined transition model. In particular, the tool provides distance approximations of surface streamlines from an attachment line and in addition, variables at the local boundary layer edge based on a three-dimensional flow field input. By assuming that the near-wall intermittency distribution given by Eq. (7) develops along the surface streamline coordinate s, a description of the intermittency distribution can be obtained *a posteriori* with the current transition model. A detailed description of the streamline length calculation algorithm is provided in Ref. [45]. An example of this application is given in Fig. 11, where field data of a laminar three-dimensional flow simulation generated by the DLR-TAU code are used as an input.

Table 4 EFTV simulation conditions

Case	*Altitude* [m]	M_e [–]	Re_u [1/m]	*AoA* [°]
243-01	28 040	7.03	$3.73 \cdot 10^6$	1.63

The geometry represents the European Flight Test Vehicle (EFTV) - a hypersonic glider model which has been designed in the framework of the HEXAFLY-INT project [46, 47] coordinated by the European Space Agency. It has a total length of 3.29 m and will be tested in a free-flight scenario where a hypersonic cruise phase at Mach 7 is planned [48]. The setup of the considered purely laminar flow simulation is given in Table 4 and aims to replicate a particular point along the scheduled trajectory, approximately 309.55s after release from the launcher.

To calculate the transition onset location, a correlation proposed by Bowcutt et al. [49] is used

$$\log_{10}(Re_{xt}) = 6.421 \exp(1.209 \cdot 10^{-4} M_e^{2.641}) \tag{19}$$

which relates the transition onset Reynolds number to the Mach number at the boundary layer edge. However, the tool offers the flexibility to choose from different onset correlations depending on the given configuration. Also note that for evaluation of the spot production parameter via Eq. (8), a free-stream turbulence level of $Tu_\infty = 0.5\,\%$ is assumed. Using the current setup, the tool predicts transitional regions on both sides of the vehicle body starting around midway along the surface. Further, no transitional regions are found on the leeward side of the wings. This is generally in line with results given in Ref. [48] where a transition assessment for the same geometry was carried out.

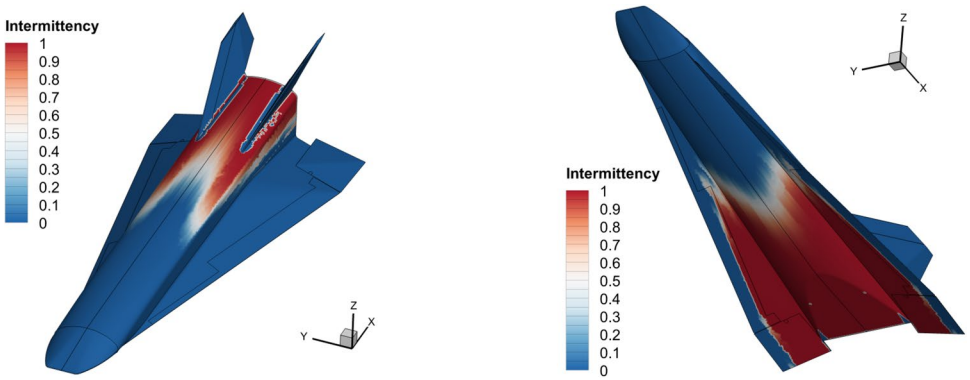

Fig. 11 Intermittency distribution on leeward (left) and windward side (right) of EFTV

6 Conclusion

In the current work, a simplified transition model was presented that uses an empirically calculated intermittency distribution to describe the transitional region. It does not involve solving a system of partial differential equations but rather blends purely laminar and turbulent solutions *a posteriori* by means of a linear combination using the intermittency as a weighting factor. The mechanisms of turbulent spot growth are incorporated by means of an empirical model which has been derived based on spot growth data from literature. Partly due to different measurement techniques and spot shape definitions, a reasonable collapse of the available data is currently not possible. Conventions regarding these aspects are required to enable a generic comparison of the data within future turbulent spot studies.

In its current version, the proposed transition model is able to capture reasonably well compressibility, Reynolds number, temperature and also pressure gradient effects on the transition rate. It has been validated for a number of test cases including zero and non-zero-pressure gradient flow and generally showed reasonable agreement with experimental data. However, a crucial limitation of the current model is its inability to predict the overshoot effect at the end of transition as it always is bound between the fully laminar and turbulent distributions.

The transition model was further applied to a full vehicle by implementing it into a previously developed boundary layer analysis tool. This allows to use best-practice correlations to obtain an approximative description of the transition zone on generic geometries. The results could be considered in the context of an initial assessment of aero-thermal loads during the design phase of high-speed vehicles. However, to explore the full potential of this extended transition tool it certainly has to be validated for a number of test cases in a future work.

Funding Open Access funding enabled and organized by Projekt DEAL.

Data Availability The datasets generated and analyzed during the current study are available from the corresponding author upon reasonable request.

Declarations

Conflict of interest The authors have no competing interests to declare that are relevant to the content of this article.

References

1. Whitehead, A.J.R.: Nasp aerodynamics. In: National Aerospace Plane Conference, p. 5013 (1989)
2. Office of the Under Secretary of Defense for Acquisition, C.: Ada board response to defense science board report. ACM SIGAda Ada Lett. **8**(4), 47–68 (1988)
3. Narasimha, R.: The laminar-turbulent transition zone in the boundary layer. Progr. Aerosp. Sci. **22**(1), 29–80 (1985)
4. Narasimha, R., Dey, J.: Transition-zone models for 2-dimensional boundary layers: A review. Sadhana **14**(2), 93–120 (1989)
5. Emmons, H.W.: The laminar-turbulent transition in a boundary layer-Part I. J. Aeronaut. Sci. **18**(7), 490–498 (1951)
6. Dhawan, S., Narasimha, R.: Some properties of boundary layer flow during the transition from laminar to turbulent motion. J. Fluid Mech. **3**(4), 418–436 (1958)
7. Solomon, W., Walker, G., Gostelow, J.: Transition length prediction for flows with rapidly changing pressure gradients. In: Turbo Expo: Power for Land, Sea, and Air, vol. 78781, pp. 001–01071. American Society of Mechanical Engineers (1995)
8. Chen, K.K., Thyson, N.A.: Extension of Emmons' spot theory to flows on blunt bodies. AIAA J. **9**(5), 821–825 (1971)
9. Adams, J., Jr.: Numerical calculation of sharp flat plate transitional and turbulent skin friction. AIAA J. **10**(6), 841–843 (1972)
10. Cebeci, T., Smith, A.M.O., Libby, P.A.: Analysis of turbulent boundary layers. (1974)
11. Steelant, J., Dick, E.: Modelling of bypass transition with conditioned Navier-Stokes equations coupled to an intermittency transport equation. Int. J. Numer. Methods Fluids **23**(3), 193–220 (1996)
12. Steelant, J., Dick, E.: Prediction of by-pass transition by means of a turbulence weighting factor: Part I—theory and validation. In: Turbo Expo: Power for Land, Sea, and Air, vol. 3. Heat Transfer; Electric Power; Industrial and Cogeneration (1999). https://doi.org/10.1115/99-GT-029 V003T01A003
13. Steelant, J., Dick, E.: Prediction of by-pass transition by means of a turbulence weighting factor: Part II—application on turbine cascades. In: Turbo Expo: Power for Land, Sea, and Air, vol. 78606, pp. 003–01004. American Society of Mechanical Engineers (1999)
14. Suzen, Y., Huang, P.: Modeling of flow transition using an intermittency transport equation. J. Fluids Eng. **122**(2), 273–284 (2000)
15. Cho, J.R., Chung, M.K.: A k-ϵ-γ equation turbulence model. J. Fluid Mech. **237**, 301–322 (1992). https://doi.org/10.1017/S0022112092003422
16. Menter, F.R., Langtry, R.B., Likki, S., Suzen, Y., Huang, P., Völker, S.: A correlation-based transition model using local variables—Part I: model formulation. J. Turbomach. **128**(3), 413–422 (2006)
17. Langtry, R.B., Menter, F.R., Likki, S.R., Suzen, Y.B., Huang, P.G., Völker, S.: A correlation-based transition model using local variables—Part II: test cases and industrial applications. J.

Turbomach. 423–434 (2004). https://asmedigitalcollection.asme.org/turbomachinery/article-pdf/doi/10.1115/1.2184353/6909185/423_1.pdf.. https://doi.org/10.1115/1.2184353
18. Van den Eynde, J., Steelant, J.: Two-equations transition model based on intermittency and empirical correlations. In: 1st International Conference on High-Speed Vehicle Science and Technology (HiSST), HiSST-2018-1300826, 26-29/11/2018, Moscow, Russia
19. Van den Eynde, J., Steelant, J., Passaro, A.: Local correlation-based transition model with phenomenological intermittency behaviour. In: 21st Int. Space Planes and Hypersonic Systems and Technology Conference, AIAA-2017-2378, 6-9 March 2017, Xiamen, China
20. Narashimha, R.: On the distribution of intermittence in the transition region of a boundary layer. J. Aeronaut. Sci. **24**, 711–712 (1957)
21. Wygnanski, I., Zilberman, M., Haritonidis, J.H.: On the spreading of a turbulent spot in the absence of a pressure gradient. J. Fluid Mech. **123**, 69–90 (1982)
22. Johnson, M.W.: Prediction of turbulent spot growth rates. In: Turbo Expo: Power for Land, Sea, and Air, vol. 78606, pp. 003–01005. American Society of Mechanical Engineers (1999)
23. Katz, Y., Seifert, A., Wygnanski, I.: On the evolution of the turbulent spot in a laminar boundary layer with a favourable pressure gradient. J. Fluid Mech. **221**, 1–22 (1990)
24. Seifert, A., Wygnanski, I.J.: On turbulent spots in a laminar boundary layer subjected to a self-similar adverse pressure gradient. J. Fluid Mech. **296**, 185–209 (1995)
25. Clark, J., Jones, T., LaGraff, J.: On the propagation of naturally-occurring turbulent spots. J. Eng. Math. **28**(1), 1–19 (1994)
26. Van den Eynde, J., Steelant, J.: Compressibility and temperature effects on turbulent spot growth. In: 1st International Conference on High-Speed Vehicle Science and Technology (HiSST), HiSST-2018-1300827, 26-29/11/2018, Moscow, Russia
27. Fischer, M.C.: Spreading of a turbulent disturbance. AIAA J. **10**(7), 957–959 (1972)
28. Chong, T.P., Zhong, S.: On the Three-Dimensional Structure of Turbulent Spots. J. Turbomach. **127**(3), 545–551 (2005). https://asmedigitalcollection.asme.org/turbomachinery/article-pdf/127/3/545/5941820/545_1.pdf. https://doi.org/10.1115/1.1928286
29. Gad-El-Hak, M., Blackwelderf, R.F., Riley, J.J.: On the growth of turbulent regions in laminar boundary layers. J. Fluid Mech. **110**, 73–95 (1981)
30. Redford, J., Sandham, N., Roberts, G.: Numerical simulations of turbulent spots in supersonic boundary layers: effects of mach number and wall temperature. Progr. Aerosp. Sci. **52**, 67–79 (2012)
31. Sandham, N.D.: Effects of compressibility and shock-wave interactions on turbulent shear flows. Flow Turbul. Combust. **97**, 1–25 (2016)
32. Jocksch, A., Kleiser, L.: Growth of turbulent spots in high-speed boundary layers on a flat plate. Int. J. Heat Fluid Flow **29**(6), 1543–1557 (2008)
33. Schubauer, G.B., Klebanoff, P.S.: Contributions on the mechanics of boundary-layer transition. Technical Report (1956)
34. Doorley, D., Smith, F.: Initial-value problems for spot disturbances in incompressible or compressible boundary layers. J. Eng. Math. **26**(1), 87–106 (1992)
35. Mayle, R.E.: The 1991 IGTI scholar lecture: the role of laminar-turbulent transition in gas turbine engines. J. Turbomach. **113**(4), 509–536 (1991). https://asmedigitalcollection.asme.org/turbomachinery/article-pdf/113/4/509/5940401/509_1.pdf. https://doi.org/10.1115/1.2929110
36. Vinod, N., Govindarajan, R.: Pattern of breakdown of laminar flow into turbulent spots. Phys. Rev. Lett. **93**(11), 114501 (2004)
37. Steelant, J., Dick, E.: Modeling of laminar-turbulent transition for high freestream turbulence. J. Fluids Eng. **123**(1), 22–30 (2001)
38. Roach, P.: The influence of a turbulent free-stream on zero pressure gradient transitional boundary layer development Part I: test cases t3a and t3b. Numer. Simul. Unsteady Flows Transit. Turbul. (1990)
39. Schülein, E.: Effects of laminar-turbulent transition on the shock-wave/boundary-layer interaction. In: 44th AIAA Fluid Dynamics Conference, p. 3332 (2014)
40. White, F.: Viscous Fluid Flow. McGraw-Hill, New York (2006)
41. Krause, M., Behr, M., Ballmann, J.: Modeling of transition effects in hypersonic intake flows using a correlation-based intermittency model. In: 15th AIAA International Space Planes and Hypersonic Systems and Technologies Conference, p. 2598 (2008)
42. Krause, M.: Numerical analysis of transition effects for scramjet intake flows. PhD dissertation, Rheinisch-Westfälische Technische Hochschule Aachen, Aachen (2010)
43. Raghunath, S., Mee, D., Narasimha, R.: Estimating turbulent spot initiation rates from transition lengths in hypersonic boundary layers. AIAA J. **55**(11), 3640–3647 (2017)
44. Wagner, A., Schramm, J.M., Hannemann, K., Whitside, R., Hickey, J.-P.: Hypersonic shock wave boundary layer interaction studies on a flat plate at elevated surface temperature. In: Shock Wave Interactions: Selected Articles from the 22nd International Shock Interaction Symposium, University of Glasgow, United Kingdom, 4-8 July 2016, pp. 231–243. Springer (2018)
45. Hoffmann, J.P., Van den Eynde, J., Steelant, J.: Boundary layer and transition onset assessment on generic geometries. In: 2nd International Conference on High-Speed Vehicle Science and Technology (HiSST), HiSST-2022-0102, 11-15/09/2022, Bruges, Belgium
46. Steelant, J., Villace, V., Kallenbach, A., Wagner, A., Andro, J.-Y., di Benedetto, S., Saracoglu, B., Chernyshev, S.L., Gubanov, A.A., Talyzin, V.A., Voevodenko, N.V., Kukshinov, N.V., Prokhorov, A.N., Grigoriev, N.V., Neely, A.J., Verstraete, D., Buttsworth, D.: Flight testing designs in hexafly-int for high-speed transportation. In: 1st International Conference on High-Speed Vehicle Science and Technology (HiSST), HiSST-2018-3101064, 26-29/11/2018, Moscow, Russia
47. Di Benedetto, S., Di Donato, M.-P., Schettino, A., Scigliano, R., Nebula, F., Morani, G., Cristillo, D., Marini, M., Cardone, S., Steelant, J., Villace, V.F.: The high-speed experimental flight test vehicle of hexafly-int: a multidisciplinary design. CEAS Space J. **13**, 291–316 (2021). https://doi.org/10.1007/s12567-020-00341-5
48. Steelant, J., Passaro, A., Fernandez-Villace, V., Gubanov, A.A., Shvalyov, Y.G., Ivanyuskhin, D.S., Voevodenko, N.V., Marini, M., di Benedetto, S.: Boundary layer transition assessment on a slender high-speed vehicle. In: 21st Int. Space Planes and Hypersonic Systems and Technology Conference, AIAA-2017-2133, 6-9 March 2017, Xiamen, China
49. Capriotti, D.: Viscous optimized hypersonic waveriders. In: 25th AIAA Aerospace Sciences Meeting, p. 272 (1987)